Biochemical Journal (2024) **481** 177–190
https://doi.org/10.1042/BCJ20230422

PORTLAND PRESS

Research Article

Leukotriene B4 receptor 1 does not mediate disease progression in a mouse model of liver fibrosis

Erin S. Coyne[1], Yilin Nie[1], Desiree Abdurrachim[2], Charlene Zhi Lin Ong[2], Yongqi Zhou[2], Asad Abu Bakar Ali[2], Stacey Meyers[1], Jeff Grein[1], Wendy Blumenschein[1], Brendan Gongol[1], Yang Liu[1], Cedric Hugelshofer[1], Ester Carballo-Jane[3] and Saswata Talukdar[1]

[1]Merck & Co., Inc., South San Francisco, CA, U.S.A.; [2]MSD, Singapore; [3]Merck & Co., Inc., Rahway, NJ, U.S.A.

Correspondence: Saswata Talukdar (saswata.talukdar@merck.com)

OPEN ACCESS

Metabolic dysfunction-associated steatohepatitis (MASH) is a prevalent liver disease that can progress to fibrosis, cirrhosis, hepatocellular carcinoma, and ultimately death, but there are no approved therapies. Leukotriene B4 (LTB4) is a potent pro-inflammatory chemoattractant that drives macrophage and neutrophil chemotaxis, and genetic loss or inhibition of its high-affinity receptor, leukotriene B4 receptor 1 (BLT1), results in improved insulin sensitivity and decreased hepatic steatosis. To validate the therapeutic efficacy of BLT1 inhibition in an inflammatory and pro-fibrotic mouse model of MASH and fibrosis, mice were challenged with a choline-deficient, L-amino acid-defined, high-fat diet and treated with a BLT1 antagonist at 30 or 90 mg/kg for 8 weeks. Liver function, histology, and gene expression were evaluated at the end of the study. Treatment with the BLT1 antagonist significantly reduced plasma lipids and liver steatosis but had no impact on liver injury biomarkers or histological endpoints such as inflammation, ballooning, or fibrosis compared to control. Artificial intelligence-powered digital pathology analysis revealed a significant reduction in steatosis co-localized fibrosis in livers treated with the BLT1 antagonist. Liver RNA-seq and pathway analyses revealed significant changes in fatty acid, arachidonic acid, and eicosanoid metabolic pathways with BLT1 antagonist treatment; however, these changes were not sufficient to impact inflammation and fibrosis endpoints. Targeting this LTB4–BLT1 axis with a small molecule inhibitor in animal models of chronic liver disease should be considered with caution, and additional studies are warranted to understand the mechanistic nuances of BLT1 inhibition in the context of MASH and liver fibrosis.

Introduction

Metabolic dysfunction-associated steatotic liver disease (MASLD) is estimated to be present in more than one-third of the global population [1,2] and the prevalence is increasing in parallel with increases in obesity and type 2 diabetes in most countries [2]. MASLD can progress from simple steatosis to more severe forms of the disease including metabolic dysfunction-associated steatohepatitis (MASH), fibrosis, cirrhosis, hepatocellular carcinoma,, and ultimately death [3–8]. A role for immune cell-driven inflammation has been characterized in the pathogenic transition from MASLD to MASH and once initiated; it is perpetuated by several intra- and extrahepatic cycles [9]. Novel therapies that can trigger the resolution of inflammation in MASH are of significant interest to the field, and although several anti-inflammatory targets have been tested in clinical trials [10–13], there are no approved therapies.

Leukotriene B4 (LTB4) is a potent pro-inflammatory lipid mediator that is produced from arachidonic acid through the sequential action of 5-lipooxygenase, 5-lipooxygenase activating protein, and leukotriene A4 hydrolase (LTA4H) [14]. LTB4 exerts well-characterized biological actions such as inducing leukocyte chemotaxis and pro-inflammatory cytokine production by signaling through its

Received: 6 October 2023
Revised: 22 November 2023
Accepted: 27 November 2023

Accepted Manuscript online: 28 November 2023
Version of Record published: 5 February 2024

Biochemical Journal (2024) 481 177–190
https://doi.org/10.1042/BCJ20230422

two G-protein coupled receptors, the high-affinity receptor Ltb4r1 (also known as BLT1) or the low-affinity receptor Ltb4r2 (also known as BLT2) [14]. Leukotriene B4 receptor 1 (BLT1) is highly expressed in immune cells such as granulocytes and macrophages and within the liver, BLT1 is expressed in hepatocytes and immune cell populations [15,16]. Although the canonical role of the LTB4–BLT1 axis is in inflammation and immune cell regulation, its role as a lipid-modulating pathway in the liver and as a potential therapeutic target for liver steatosis and insulin resistance has been reported [15,17–19]. However, the mechanisms through which this pathway modulates lipid metabolism are still unclear. Global deletion of Ltb4r1 in mice results in decreased levels of alanine transaminase (ALT) and decreased liver fat content when mice are fed a high-fat diet [18] while hepatocyte-specific knockout of Ltb4r1 in mice results in decreased levels of ALT, aspartate transaminase (AST), hepatic fat, and lipogenic gene expression [15]. Additionally, a small molecule antagonist of BLT1 is sufficient to reduce hepatic steatosis and lipogenic gene expression in mice fed a high-fat diet [17] and reduce circulating and hepatic triglycerides in db/db mice [15]. Moreover, a recent clinical trial was initiated, and subsequently discontinued, for LYS006 (LTA4H inhibitor), alone or in combination with tropifexor for the indication of MASH (ClinicalTrials.gov, NCT04147195) demonstrating the significant investment that has been made to evaluate the therapeutic potential of targeting the LTB4–BLT1 axis in chronic liver disease.

In this report, to extend the previous findings on BLT1 loss of function biology to MASH, liver fibrosis, and late-stage liver disease, a small molecule BLT1 antagonist [20,21] was used to inhibit LTB4 action on BLT1 receptors in a mouse model of MASH and liver fibrosis induced by a choline-deficient, L-amino acid-defined, high-fat diet (CDAA–HFD). This model recapitulates progressive steatohepatitis and the development of MASH-induced fibrosis and indeed, clinical candidates such as pan peroxisome proliferator-activated receptor agonist lanifibranor, can significantly reduce liver steatosis, inflammation, and fibrosis in this model [22]. Primary endpoints in clinical trials for MASH include MASH resolution without worsening of fibrosis and/or one-stage fibrosis improvement without worsening of MASH. These regulatory endpoints are assessed by histology as defined by the MASH Clinical Research Network (CRN) [23,24] and include components such as steatosis, inflammation, hepatocyte ballooning, and liver fibrosis. In this report, we demonstrate that inhibition of BLT1 in the CDAA–HFD model results in decreased hepatic steatosis and circulating lipids, consistent with previous findings [15,17,18]. Moreover, RNA-seq and gene ontology enrichment analysis reveals that inhibition of BLT1 results in changes in arachidonic acid, eicosanoid, and fatty acid metabolism. However, in this model, inhibition of BLT1 has no effect on liver injury biomarkers and no effect on the histological components of regulatory endpoints including inflammation, hepatocyte ballooning, and liver fibrosis. These findings suggest that while BLT1 inhibition has beneficial effects on lipid metabolism and liver steatosis in multiple preclinical disease models, in highly inflammatory and pro-fibrotic disease models, BLT1 inhibition is not sufficient to delay or reverse the effects of inflammation and fibrosis.

Results

Inhibition of BLT1 reduces plasma lipids but has no effect on liver injury biomarkers in the CDAA–HFD model

Previous work has demonstrated that inhibition of BLT1 with a small molecule antagonist is protective against the development of lipid accumulation in the liver [17]. To extend these findings to a more inflammatory and fibrotic model of liver disease, we challenged mice with a CDAA–HFD, a well-established model to study chronic liver disease. After 4 weeks on diet, mice were treated with a BLT1 antagonist (BLT1i) that has an EC50 of <100 nM in the BLT1 cAMP assay, and a favorable selectivity profile over BLT2 (>100×). The compound shows good kinetic solubility across pH ranges (>100 μM), as well as high permeability. The mouse pharmacokinetic profile exhibits low clearance, long half-life (>2 h), and high oral bioavailability (>50%) [20,21]. BLT1i was formulated into the diet such that the animals received a daily dose of 30 or 90 mg/kg for 8 additional weeks (Figure 1A). We observed a 10% decrease in body weight as well as a decrease in food intake in the group receiving the 90 mg/kg dose of BLT1i (Supplementary Figure S1A,B). Upon CDAA–HFD feeding, we observed a significant downregulation of Ltb4r1 and Ltb4r2 expression in the liver with no changes in Lta4h expression, and treatment with BLT1i had no further effect on the expression of Ltb4r1, Ltb4r2, or Lta4h (Supplementary Figure S2). The circulating level of BLT1i at the terminal time point was sufficient to achieve up to 75% inhibition based on previously characterized CD11b neutrophil inhibition assays with this compound and higher plasma exposure was observed with increasing doses of BLT1i (Supplementary Figure S2D,

Biochemical Journal (2024) **481** 177–190
https://doi.org/10.1042/BCJ20230422

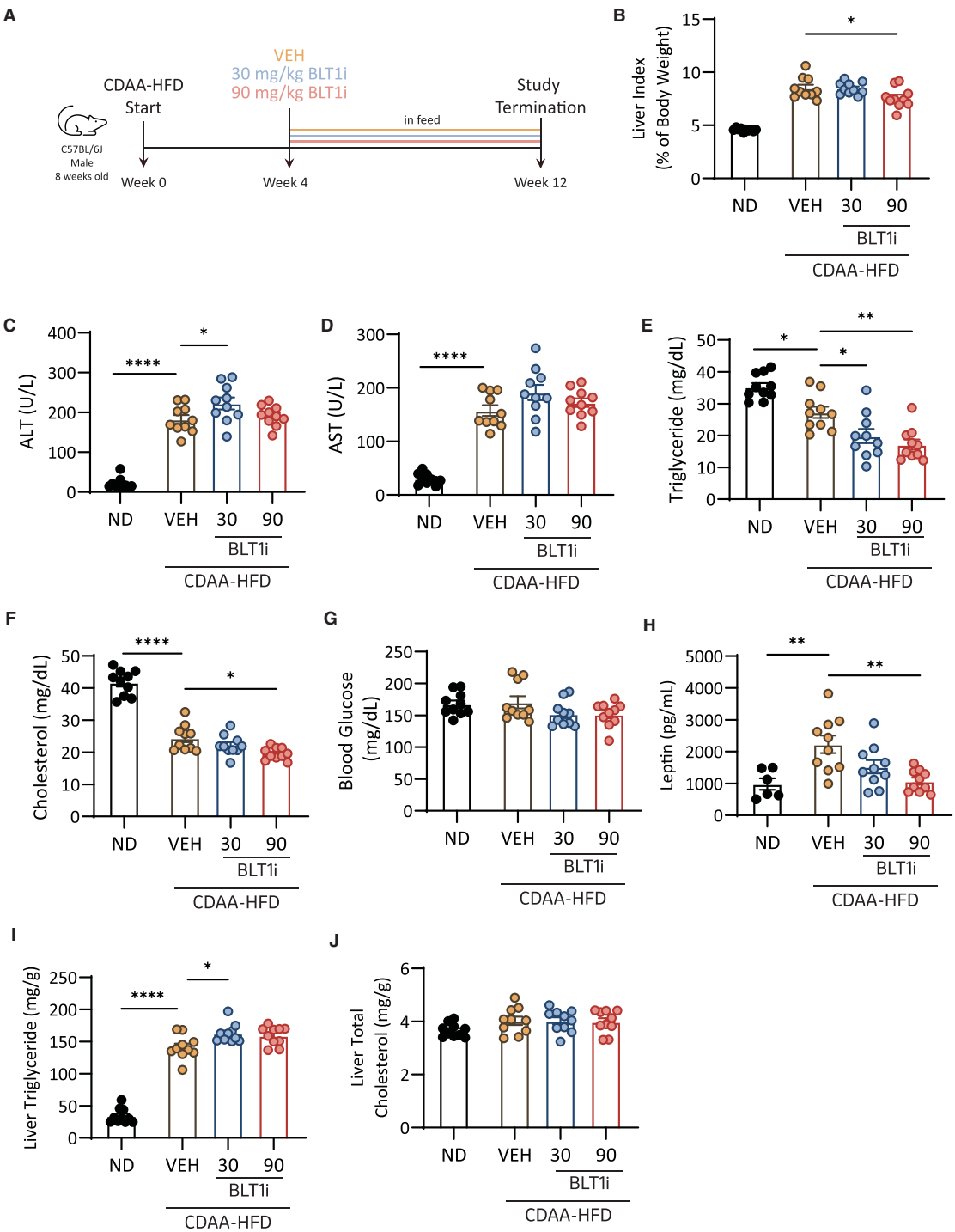

Figure 1. Inhibition of BLT1 reduces plasma lipids but has no effect on liver injury biomarkers in the CDAA–HFD model of MASH and liver fibrosis.

(**A**) Schematic of study design. Mice were fed a CDAA–HFD or normal chow diet for 4 weeks after which the CDAA–HFD was formulated with a BLT1 antagonist (BLT1i) to generate a daily dose of 30 or 90 mg/kg. After 8 additional weeks on compound formulated diet, the study was terminated. (**B**) Liver index of liver weight as a percentage of body weight. Study endpoint blood plasma analysis of (**C**) ALT, (**D**) AST, (**E**) triglycerides, (**F**) cholesterol, (**G**) glucose, and (**H**) leptin levels. Liver levels of (**I**) triglycerides and (**J**) total cholesterol normalized to grams of liver tissue. ND, normal diet; VEH, vehicle. Data are presented as mean ± SEM. $n = 9–10$ per group. Compared with CDAA–HFD VEH $^{*}P < 0.05$, $^{**}P < 0.01$, $^{****}P < 0.0001$.

Biochemical Journal (2024) **481** 177–190
https://doi.org/10.1042/BCJ20230422

E). As expected, mice fed a CDAA–HFD had a significantly increased liver index (liver weight as a percentage of body weight) compared with mice fed a normal diet, and treatment with BLT1i at 90 mg/kg was sufficient to significantly decrease the liver index compared with the vehicle group (Figure 1B). Both ALT and AST activities were significantly increased in mice fed the CDAA–HFD and treatment with BLT1i at 30 mg/kg further increased ALT activity but there was no effect on ALT or AST activity in the 90 mg/kg BLT1i group compared with the vehicle control (Figure 1C,D). Since hepatic steatosis can be driven by a number of factors such as aberrant lipid and glucose metabolism, we assessed levels of circulating lipids, glucose, and leptin. Plasma lipids, including triglycerides and total cholesterol, were significantly decreased in mice fed the CDAA–HFD, and treatment with BLT1i further reduced triglycerides and total cholesterol levels (Figure 1E,F). Fasting blood glucose levels were unchanged between treatment groups (Figure 1G) while leptin levels were significantly decreased with 90 mg/kg BLT1i treatment (Figure 1H). Liver triglyceride levels were significantly increased in mice fed the CDAA–HFD, and a further increased in liver triglycerides was observed in the 30 mg/kg treated group while no significant difference was observed in the 90 mg/kg treated group (Figure 1I). Liver cholesterol levels were unchanged between treatment groups (Figure 1J). Since we observed a significant decrease in body weight in the 90 mg/kg BLT1i treatment group that may confound the results, we performed a multivariable ANCOVA analysis using body weight as a covariate. For dependent variables that were significantly affected by treatment (plasma triglycerides, cholesterol, leptin), we found that treatment alone, not body weight, was a significant predictor of effect on the dependent variable. Together, this data suggests that inhibition of BLT1 has effects on lipid metabolism but not on liver injury biomarkers in this diet model.

Inhibition of BLT1 has no effect on MASLD activity score but decreases steatosis area in the CDAA–HFD model

Next, we wanted to assess if MASLD activity score (MAS) histopathological features such as steatosis, inflammation, and hepatocyte ballooning were changed upon BLT1i treatment in the CDAA–HFD model. Liver sections were stained with hematoxylin and eosin (H&E), evaluated by a histopathologist, and scored based on the MASH CRN scoring system [23,24]. H&E staining revealed a dramatic increase in lipid droplets and inflammatory foci in the liver of mice fed the CDAA–HFD (Figure 2A). However, there was no significant effect of BLT1i on MAS (Figure 2B), and its individual components steatosis (Figure 2C), inflammation (Figure 2D), and ballooning (Figure 2E) scores. Since the steatosis score in each group had reached the maximum score of 3 out of 3 in this aggressive model of MASH and liver fibrosis, we wanted to ascertain more granular insight into histopathological features including characterizing lipid droplet size as well as the zonal distribution of steatosis within the three zones (portal tract (PT), perisinusoidal (PS), central vein (CT)) of the liver lobule using artificial intelligence (AI)-powered digital pathology [25]. We found that there was a significant decrease in steatosis in all zones of the liver including the zone 1 PT region, zone 2 PS region, zone 3 CV region in the 90 mg/kg BLT1i group compared with vehicle control (Figure 2F). This decrease in steatosis in all zones observed in the BLT1i treatment arm amounted to a 21% total decrease in steatosis area compared with vehicle control. Finally, using AI-powered digital pathology, we assessed whether there was a shift in lipid storage from large lipid droplets, or macrosteatosis, to smaller lipid droplets, or microsteatosis, in the BLT1i treated mice. Indeed, we observed a significant decrease in macrosteatosis, with a trend toward increasing microsteatosis in the 90 mg/kg BLT1i treatment group compared with vehicle control (Figure 2G). In addition, we used AI-powered digital pathology to quantify the inflammatory cell density in the liver and found there was a significant upregulation in inflammatory cell density in the CDAA–HFD VEH treated group, but there was no significant difference in inflammatory cell density upon BLT1i treatment (Figure 2H). Taken together this data demonstrates that BLT1 inhibition can significantly decrease liver steatosis, specifically macrosteatosis, but not inflammatory cell recruitment and underscores the importance of sufficient granularity in the analysis of liver histopathological features.

Inhibition of BLT1 has no effect on lipogenic or inflammatory gene expression in the CDAA–HFD model

To further characterize the effect of BLT1 inhibition on decreasing steatosis, we assessed the expression of genes associated with lipid synthesis and storage. Mice fed the CDAA–HFD had significantly decreased expression of genes involved in *de novo* lipogenesis and fatty-acid esterification, but we did not observe a significant effect of BLT1i treatment on the expression of these genes compared with the vehicle control group (Figure 3A, B). In addition to genes involved in lipid metabolism, we assessed genes involved in pro- and anti-

Biochemical Journal (2024) **481** 177–190
https://doi.org/10.1042/BCJ20230422

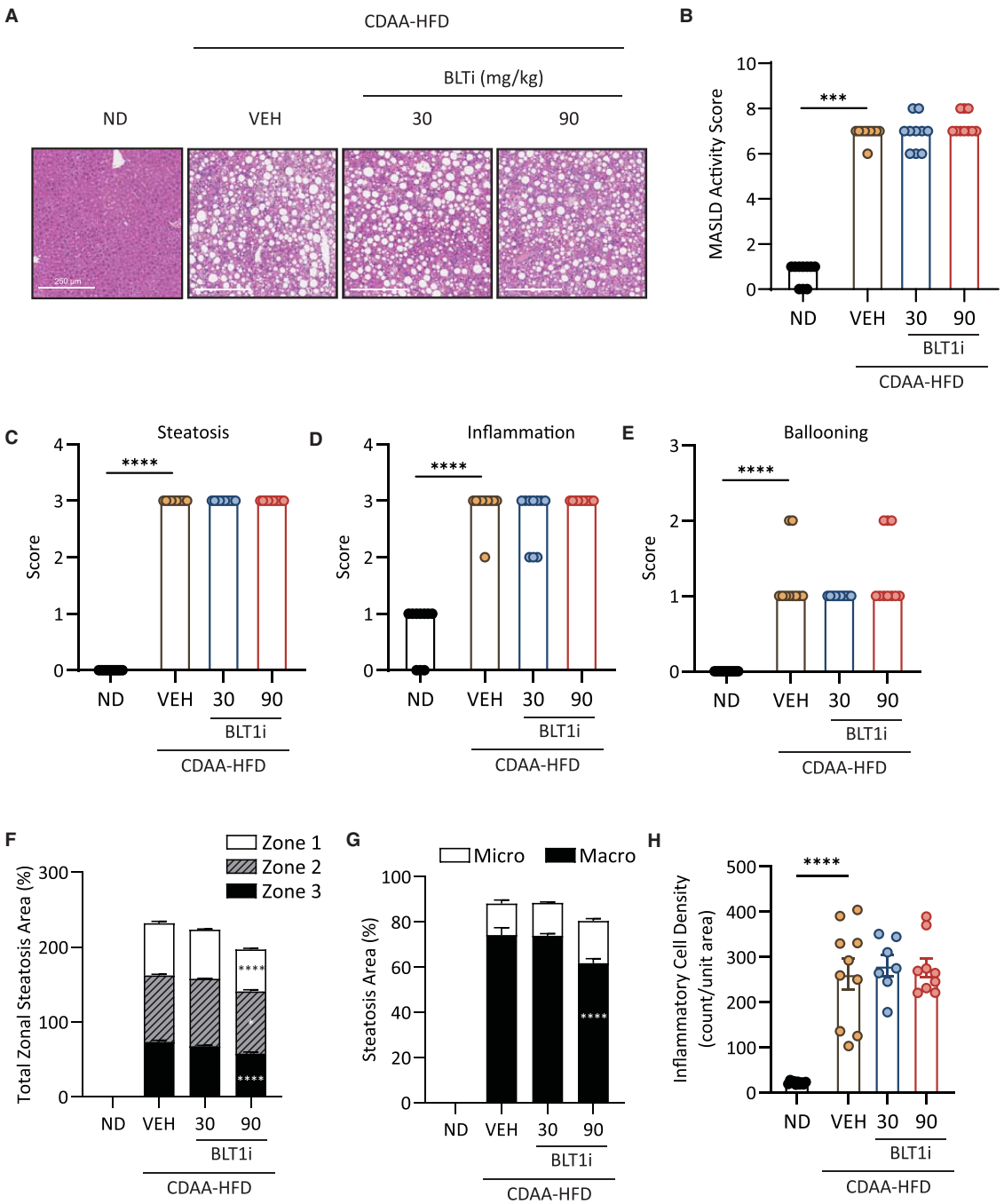

Figure 2. Inhibition of BLT1 has no effect on MASLD activity score but decreases steatosis area in the CDAA–HFD model of MASH and liver fibrosis.

(**A**) Representative images of H&E-stained liver sections from mice fed a normal diet or CDAA–HFD and treated with BLT1i. (**B**) Pathologist scored MASLD activity score. (**C–E**) Pathologist scored components of MASLD activity score (**C**) steatosis, (**D**) inflammation, and (**E**) hepatocyte ballooning. (**F**) Artificial intelligence (AI)-guided digital pathology analysis and quantification of steatosis area by liver zones — zone 1 portal tract (PT), zone 2 perisinusoidal region (PS), zone 3 central vein (CV) — represented as percent area of each liver zone. (**G**) AI-guided quantification of total area of macrosteatosis and microsteatosis. (**H**) AI-guided quantification of inflammatory cell density. ND, normal diet; VEH, vehicle. Data are presented as mean ± SEM. *n* = 9–10 per group. Compared with CDAA–HFD VEH $^{*}P < 0.05$, $^{***}P < 0.001$, $^{****}P < 0.0001$.

Biochemical Journal (2024) **481** 177–190
https://doi.org/10.1042/BCJ20230422

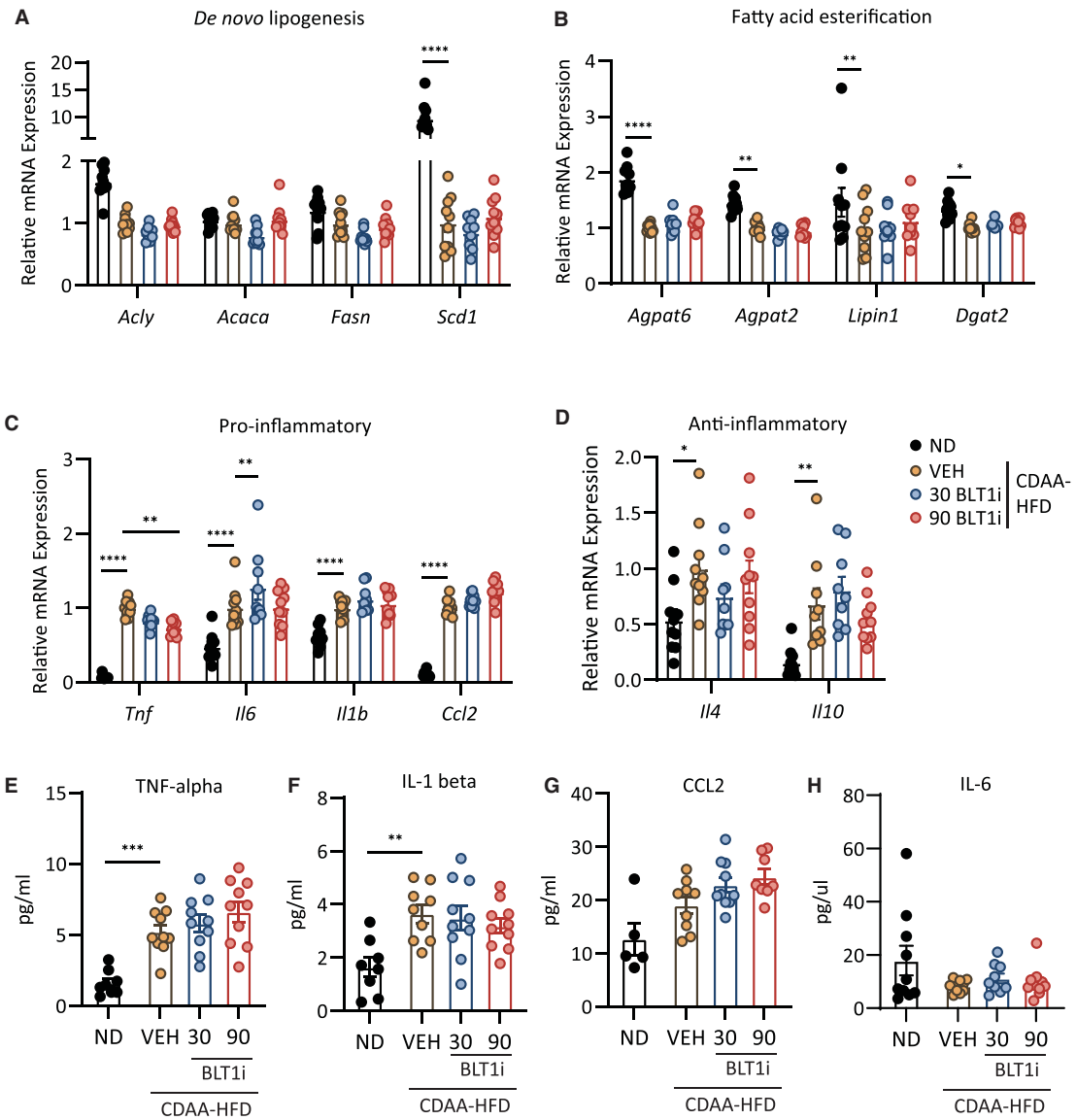

Figure 3. Inhibition of BLT1 has no effect on liver lipogenic or inflammatory gene expression in the CDAA–HFD model of MASH and liver fibrosis.

(**A,B**) Relative mRNA expression of genes involved in (**A**) *de novo* lipogenesis and (**B**) fatty acid esterification in liver of mice on CDAA–HFD treated with BLT1i. (**C,D**) Relative mRNA expression of (**C**) pro-inflammatory and (**B**) anti-inflammatory genes in liver of mice on CDAA–HFD treated with BLT1i. (**E–H**) Circulating levels of pro-inflammatory cytokines from plasma at study endpoint. (**E**) TNF-alpha, (**F**) IL-1 beta, (**G**) CCL2, and (**H**) IL-6. ND, normal diet; VEH, vehicle. $n = 9–10$ per group. Data are presented as mean ± SEM. $n = 9–10$ per group. Compared with CDAA–HFD VEH $^{*}P < 0.05$, $^{**}P < 0.01$, $^{***}P < 0.001$, $^{****}P < 0.0001$.

inflammatory processes. We observed a significant increase in pro- and anti-inflammatory gene expression in mice fed the CDAA–HFD (Figure 3C,D). Treatment with BLT1i significantly decreased the expression of tumor necrosis factor-alpha (*Tnf*) gene expression at the 90 mg/kg dose but increased the expression of interleukin 6 (*Il6*) at the 30 mg/kg dose of BLT1i (Figure 3C). In addition, treatment with BLT1i had no effect on anti-inflammatory cytokine gene expression in the liver of mice fed a CDAA–HFD (Figure 3D). Since we did not observe an effect on inflammatory gene expression in the liver and BLT1i will be active in extrahepatic tissues, we assessed the levels of circulating pro- and anti-inflammatory cytokines. We observed an increase in TNF (Figure 3E), IL1B (Figure 3F), and CCL2 (Figure 3G) and a decrease in IL6 (Figure 3F) in the plasma of mice fed the CDAA–HFD however BLT1i treatment had no effect on the levels of these circulating

pro-inflammatory cytokines (Figure 3E–H). Anti-inflammatory cytokines IL-4 and IL-10 were below the limit of detection in the circulation. Together, this data indicates that treatment with BLT1i has no effect on lipogenic and inflammatory gene expression in the liver and no effect on circulating pro-inflammatory cytokines at this timepoint in the CDAA–HFD model.

Inhibition of BLT1 has no effect on liver fibrosis in the CDAA–HFD model

To evaluate the effect of BLT1 inhibition on later stages of liver disease, we assessed the effect of BLT1i treatment on fibrosis endpoints. Picrosirius red (PSR) staining of the livers revealed a significant deposition of collagen in the livers of mice fed the CDAA–HFD (Figure 4A). Pathologist scoring of the livers using MASH CRN fibrosis criteria revealed a significant increase in CRN fibrosis score upon CDAA–HFD but no significant difference between vehicle and BLT1i treated groups (Figure 4B). Similarly, quantification of the PSR-stained area showed a sixfold increase in PSR staining on the CDAA–HFD fed mice compared with normal diet, but there was no significant difference between vehicle and BLT1i treated groups (Figure 4C). We next assessed the gene expression levels of genes important in the development of fibrosis including various collagens and alpha smooth muscle actin. We observed a significant upregulation of *Col1a1*, *Col3a1*, and *Acta2* upon CDAA–HFD feeding and BLT1i treatment had no impact on the expression of these genes (Figure 4D). Since we previously established the need for increased granularity to assess histopathological features (Figure 2), we used AI-powered digital pathology to assess liver fibrosis in more detail. First, we assessed whether the zonal distribution of fibrosis was different upon treatment with BLT1i. We did not observe any significant difference in fibrosis in any of the liver zones upon BLT1i treatment (Figure 4E). Finally, we assessed the extent to which fibrosis is co-localized with steatosis, the regression of which is predicted to be associated with better clinical outcomes [26]. We observed that in the high-dose BLT1i group, there was significantly less steatosis co-localized fibrosis compared with the vehicle control group which may be due, in part, to decreased overall steatosis (Figure 4F).

Transcriptomics analysis reveals treatment with BLT1 antagonist modulates arachidonic acid, fatty acid, and eicosanoid metabolic pathways

To further understand how BLT1 inhibition modulates lipid metabolism and steatosis while having no effect on inflammation or fibrosis in this model, we performed transcriptomics analysis on the liver from CDAA–HFD fed mice treated with vehicle or 90 mg/kg BLT1i. Principal component analysis (PCA) analysis revealed a distinct separation between vehicle and BLT1i treated groups (Figure 5A). Differential gene expression analysis identified 77 significantly upregulated and 17 significantly down-regulated genes upon 90 mg/kg BLTi treatment (Figure 5B,C). Pathway analyses were performed, and arachidonic acid, fatty acid, and eicosanoid metabolic pathways were identified as significantly altered with BLT1i treatment (Supplementary Figure S3). Further analysis by qPCR of several of the most abundantly upregulated genes including cytochrome P450, family 4, subfamily a, polypeptide 14 (*Cyp4a14*), growth differentiation factor 15 (*Gdf15*), early growth response 1 (*Egr1*), and enoyl-CoA hydratase/3-hydroxyacyl CoA dehydrogenase (*Ehhadh*) revealed a dose–responsive increase in gene expression with increasing BLT1 inhibition suggesting a specific effect of BLT1 inhibition on the expression of these genes (Figure 5D–G). Consistent with the known function of these genes in the liver, the increased expression upon inhibition of BLT1 would result in significant alterations in lipid metabolism.

Discussion and conclusion

There are currently no approved therapies for MASH or liver fibrosis and while new classes of weight loss drugs are certain to provide some benefit to the liver, there remains an unmet clinical need for treatments targeting late-stage liver disease. Lobular inflammation is a key feature of MASH and evidence suggests that the transition to the inflammatory state is a major driver of disease pathogenesis. Therapeutic interventions that modulate inflammation could have a significant impact on disease progression. Indeed, several anti-inflammatory therapies have made it to late-stage clinical trials including Cenicriviroc (CCR2/CCR5), Selonsertib (ASK1), and Simtuzumab (LOXL2), but have failed to meet primary endpoints [11–13] revealing the complex nature of inflammation in chronic liver disease. At present, the successful translation of anti-inflammatory therapies to the treatment of MASH in the clinic has proven challenging, necessitating the evaluation of novel pathways and mechanisms in the pathogenesis of inflammation in chronic liver disease. Novel

Biochemical Journal (2024) **481** 177–190
https://doi.org/10.1042/BCJ20230422

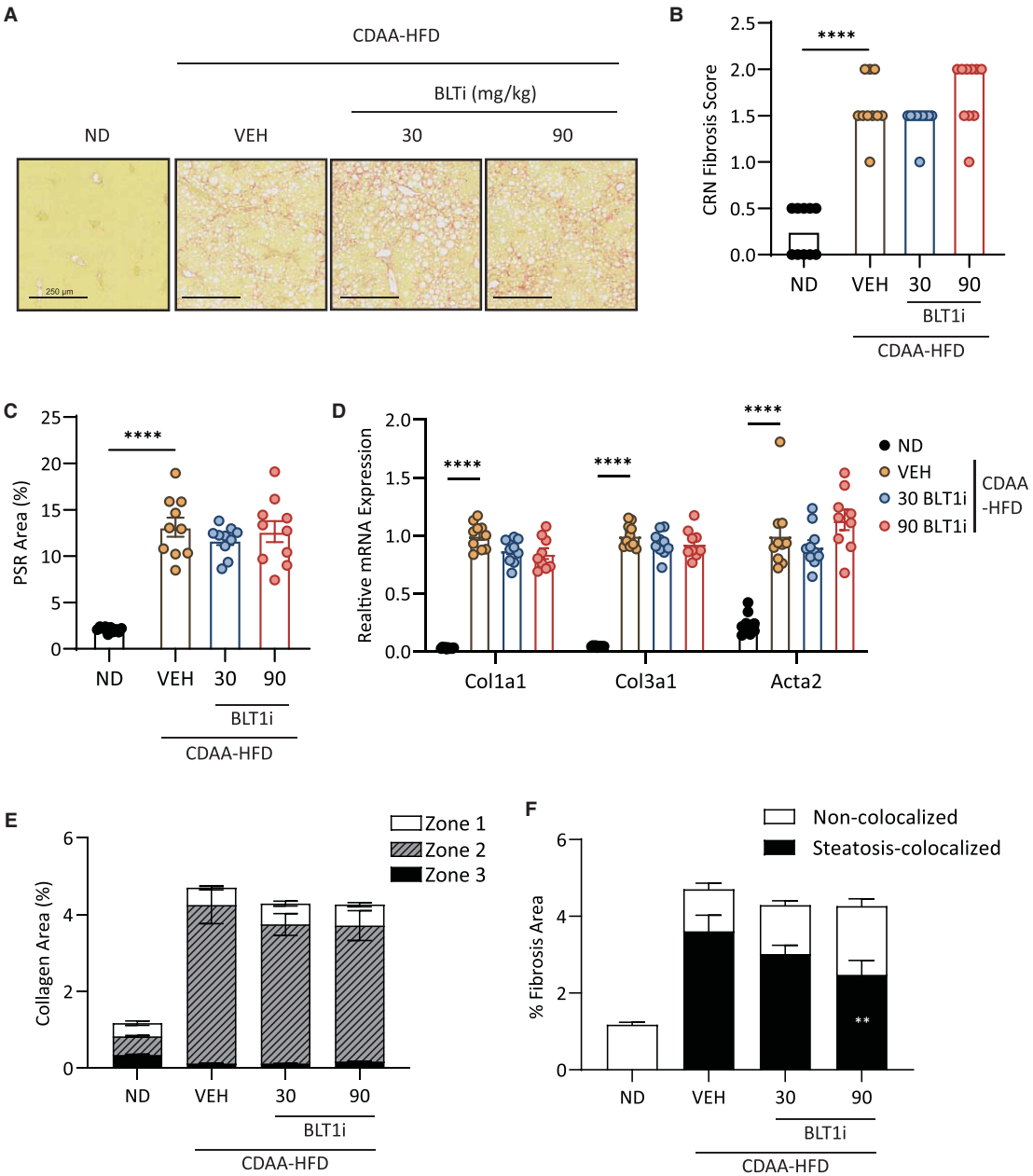

Figure 4. Inhibition of BLT1 has no effect on liver fibrosis in the CDAA–HFD model.

(**A**) Representative images of picrosirius red stained liver sections from mice fed a normal diet or CDAA–HFD and treated with vehicle or BLT1i. (**B**) Pathologist scored CRN fibrosis score. (**C**) Quantification of whole-slide images of Picrosirius red stained area represented as percentage of total area. (**D**) Relative mRNA expression of fibrosis-associated genes Col1a1, Col3a1, and Acta2. (**E**) AI-powered digital pathology analysis and quantification of SHG collagen area by liver zones — Zone 1 portal tract (PT), Zone 2 perisinusoidal region (PS), Zone 3 central vein (CV). (**F**) AI-powered digital pathology analysis of the co-localization of fibrosis with steatosis regions. ND, normal diet; VEH, vehicle. Data are presented as mean ± SEM. $n = 9–10$ per group. Compared with CDAA–HFD VEH $^{*}P < 0.05$, $^{**}P < 0.01$, $^{****}P < 0.0001$.

therapies, such as BLT1 antagonism, that could trigger the resolution of inflammation in MASH would be valuable.

In this report, to interrogate whether disrupting the pro-inflammatory LTB4–BLT1 axis by pharmacological inhibition of BLT1 using a small molecule inhibitor provides a therapeutic benefit in the pathogenesis of

Biochemical Journal (2024) **481** 177–190
https://doi.org/10.1042/BCJ20230422

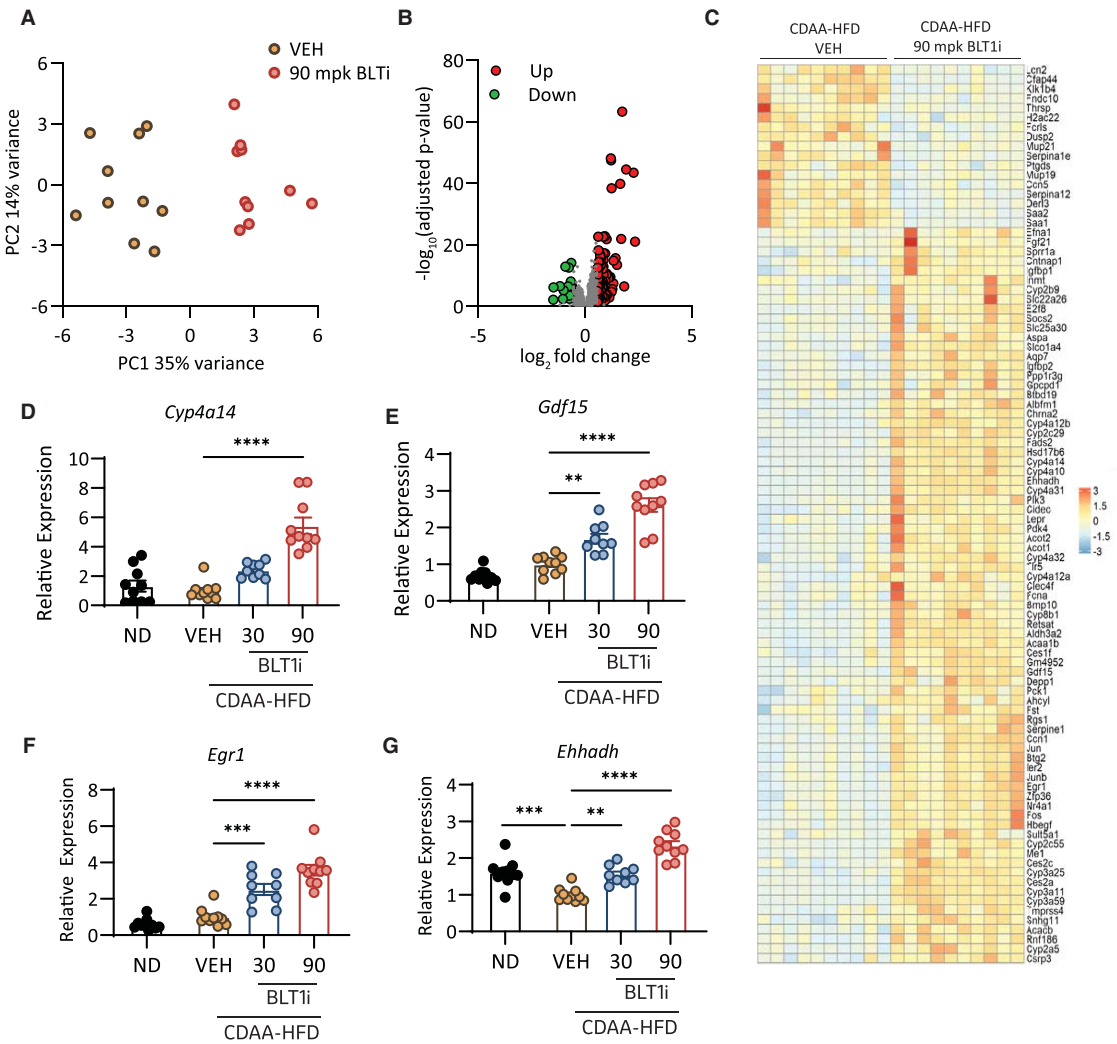

Figure 5. Transcriptomics analysis reveals treatment with BLT1 inhibitor modulates arachidonic acid, fatty acid, and eicosanoid metabolic pathways.

RNA sequencing was performed on RNA from vehicle and BLT1i (90 mg/kg) treated livers. (**A**) Principal component analysis of samples. (**B**) Volcano plot of differentially regulated genes. Significantly upregulated genes are shown in red and significantly down regulated genes in green. Significance was defined as an FDR adjusted *P*-value <0.05. (**C**) Heat map and clustering of differentially expressed genes across all 20 samples represented as column scaled normalized count values. (**D–G**) Relative mRNA expression of top hits from transcriptomics analysis. (**D**) *Cyp4a14*, (**E**) *Gdf14*, (**F**) *Egr1*, and (**G**) *Ehhadh* expression in liver from mice fed a normal diet or CDAA–HFD and treated with BLT1i. ND, normal diet; VEH, vehicle. Data are presented as mean ± SEM. $n = 9–10$ per group. Compared with CDAA–HFD VEH $^{*}P < 0.05$, $^{**}P < 0.01$, $^{***}P < 0.001$, $^{****}P < 0.0001$.

MASH, fibrosis, and late-stage liver disease, we tested a BLT1 antagonist in the well-characterized CDAA–HFD mouse model which induces a robust inflammatory and fibrotic response within as little as 6 weeks [27]. In this model, we examined MASH CRN histological endpoints and found that inhibition of BLT1 does not reduce liver inflammation or fibrosis. We did, however, demonstrate an effect of BLT1 inhibition on reducing liver steatosis measured by AI-guided digital pathology, confirming findings from previous studies, and suggesting that the LTB4–BLT1 axis modulates lipid metabolism pathways in various metabolic models. Unlike previous reports [15,17,18], we did not observe a significant decrease in liver injury biomarkers ALT or AST, or a decrease in circulating pro-inflammatory modulators but we did observe a significant decrease in plasma lipids including triglycerides and total cholesterol.

Biochemical Journal (2024) **481** 177–190
https://doi.org/10.1042/BCJ20230422

Liver transcriptomics and gene ontology enrichment analysis revealed that inhibition of BLT1 resulted in altered arachidonic acid, eicosanoid, and fatty acid metabolism. Since the ligand for BLT1, LTB4, is an arachidonic acid derivative, it is possible that inhibition of BLT1 is driving a feedback loop to regulate arachidonic acid and eicosanoid metabolism, but this remains to be explored. Several of the top hits from the analysis were genes that have already been implicated in the pathogenesis of chronic liver disease including *Cyp4a14*, *Gdf15*, and *Egr1*. In this study, these genes were all upregulated in response to BLT1 inhibition in a dose-dependent manner (Figure 5). Previous work demonstrated that in three distinct mouse models of MASLD, overexpression of *Cyp4a14* resulted in a fatty liver phenotype whereas gene disruption attenuated liver lipid accumulation [28]. On the other hand, in cholestatic liver disease, *Cyp4a14* gene deficiency aggravated, whereas its overexpression ameliorated, bile-duct ligation-induced hepatic fibrosis [29] revealing both hepatoprotective and hepatotoxic effects of *Cyp4a14* in different models of liver disease. Interestingly, depletion of *Egr1*, another gene upregulated by BLT1i treatment, was protective against lipid accumulation and fibrosis in the liver in a db/db mouse model [30]. Together these studies suggest that upregulation of *Cyp4a14* and *Egr1*, as seen with inhibition of BLT1 in this study, would lead to increased lipid accumulation and fibrosis inconsistent with our results. However, as with *Cyp4a14*, *Egr1* may have context-dependent effects in different models of disease. Gdf15 was also significantly upregulated in response to BLT1 inhibition. Previous studies have shown that Gdf15 gene deficiency resulted in aggravated MASH phenotypes while overexpression attenuated these same phenotypes and improved lipid homeostasis [31,32] suggesting that induction of *Gdf15* expression may be hepatoprotective and consistent with the findings in this study. How LTB4 signaling through BLT1 modulates the expression of these genes remains to be explored.

There are several reasons why the results of this study may conflict with other published reports. First, different models to induce MASH and liver fibrosis have been used across studies. Most prior studies testing the effect of loss of BLT1 used high-fat diets or genetic models of obesity to induce inflammation, insulin resistance, and liver steatosis and these models, at the timepoints tested, are not sufficient to induce significant liver fibrosis [27,33] whereas livers in the CDAA–HFD model rapidly develop robust inflammation and fibrosis [27]. Second, we used stringent histological endpoints developed by the MASH CRN to evaluate the pathogenesis of MASH and fibrosis in our model whereas other studies use liver injury biomarkers, liver lipid content, and gene expression as surrogates to assess liver pathology [15,17,18]. Finally, we assessed a specific time point in the CDAA–HFD model (Figure 1A) chosen for its high levels of inflammation and fibrosis, so it is possible that the window where the impact of BLT1i treatment on inflammation and fibrosis endpoints was not captured in this study. However, we also assessed an earlier time point with lower disease burden in this model and similarly, observed no effect of BLT1i treatment on inflammatory or fibrotic liver endpoints (data not shown). It is also possible that the CDAA–HFD model is not the optimal model to test the effects of BLT1 inhibition due to the dysregulated lipid metabolism as a result of dietary choline deficiency. Nonetheless, we demonstrate in this well-characterized and commonly used CDAA–HFD model of MASH and fibrosis, that inhibition of BLT1 is not sufficient to reduce inflammation or fibrosis.

Our report reveals a significant disconnect between changes in lipid metabolism/steatosis and inflammation/fibrosis upon BLT1 inhibition. Although MASLD is considered a progressive disease beginning with metabolic dysfunction and steatosis that leads to inflammation, hepatocyte degeneration, and ultimately, fibrosis and cirrhosis, only a fraction of those with simple steatosis will progress to MASH and beyond. The transition from simple steatosis to MASH is a complex and dynamic process that involves both extra and intrahepatic pathways and although many mechanisms in this process have been elucidated it is still not well understood [34]. Like BLT1 inhibition in this model, it is not unprecedented for an intervention that protects on steatosis endpoints to have no effect on fibrosis endpoints. For example, in a clinical trial assessing the efficacy and safety of pioglitazone, vitamin E, or placebo in patients with MASH, the authors found that treatment with both pioglitazone and vitamin E was associated with significant reductions in hepatic steatosis, but neither treatment was associated with improvement in fibrosis scores [35]. Further studies to elucidate the effects of the LTB4–BLT1 axis in different mouse models of MASH and liver fibrosis are necessary to understand the disconnect between lipid metabolism, inflammation, and fibrosis with BLT1 inhibition.

Ultimately, pharmacological inhibition of BLT1 may not be the optimal approach for treating MASH, fibrosis, and late-stage liver disease but further exploration of the pathway is warranted to better understand the biology of the LTB4-BLT1 axis in the liver. Disruption of the LTB4-BLT1 axis could be a useful tool to further characterize the disconnect between steatosis and downstream sequelae.

Biochemical Journal (2024) 481 177–190
https://doi.org/10.1042/BCJ20230422

Materials and methods

Animal studies

Animal experiments were conducted in accordance with the Public Health Service Policy on Human Care and Use of Laboratory Animals from the Office of Laboratory Animal Welfare, and the Guide for the Care of Use of Laboratory Animals from the National Research Council. All experiments were approved by the Institution Animal Care and Use Committee of Merck & Co., Inc., South San Francisco, CA, U.S.A., and were performed in accordance with relevant guidelines and regulations at MRL South San Francisco. All mice were housed in a temperature and humidity-controlled environment with a 12-h light–dark cycle, environmental enrichment, and ad libitum access to food and water. Male C57BL/6J mice from Jackson Laboratory were used for all studies. At 8 weeks of age, mice were randomized into four groups with equivalent body weights and were fed a normal chow laboratory diet (LabDiet, #5001) or a CDAA–HFD with 60 kcal% fat with 0.1% methionine and no added choline (Research Diets, A06071302). After 4 weeks, one group remained on the chow diet, one group remained on CDAA–HFD, one group was started on CDAA–HFD with a 30 mg/kg dose of BLT1i, and the final group was started on CDAA–HFD with a 90 mg/kg dose of BLT1 antagonist (BLT1i) for the final 8 weeks of the study (Figure 1A). BLT1 antagonist was formulated into the feed at a concentration sufficient to produce a daily dose of 30 or 90 mg/kg based on known daily feeding behavior. Mice were anesthetized using isoflurane prior to terminal exsanguination followed by bilateral thoracotomy.

CD11b neutrophil assay

Whole blood was collected from mice treated with vehicle, 1, 3, 10, or 30 mg/kg BLT1i after 1, 6, or 24 h. LTB4 was added to blood at a final concentration of 20 nM and incubated at 37°C for 10 min. Cells were stained with an antibody cocktail (Supplementary Table S1) for 30 min at 4°C, washed, and then flow cytometry analysis was performed. Cells were gated on granulocytes (LY6G+) and CD66b+ cells were identified as neutrophils. CD11b staining within the CD66b+ population was quantified to assess BLT1 activity.

Plasma and tissue analysis

Blood was collected from animals at the 12-week terminal timepoint by cardiac puncture and transferred into K2-EDTA tubes following a 5 h fast. ALT, AST, total cholesterol, and triglycerides were measured using the cobas c 311 Clinical Analyzer (Roche, Indianapolis, IN, U.S.A.). Blood glucose was measured from whole blood using the AlphaTrak2 blood glucose monitor after a 5 h fast at the 12-week study timepoint. Plasma cytokines and chemokines were analyzed using the Immune Monitoring 48-Plex Mouse ProcartaPlex™ Panel (Thermo Fisher Scientific, Waltham, MA, U.S.A.) per the manufacturer's protocol. For liver lipid analysis, ∼100 mg of tissue was homogenized in 5% IGEPAL CA-630, heated to 80–100°C twice, centrifuged, and the extracted lipids from the supernatant were measured using the cobas c 311 Clinical Analyzer.

Histology and pathology

Liver was fixed, embedded in paraffin, sectioned, and stained with H&E and PSR. All stained slides were examined by light microscopy and digital scanned at 20× brightfield. MASH CRN scoring system was used by a pathologist to obtain an MAFLD activity score and fibrosis score. PSR stained area was quantified using whole slide image analysis. Samples were blinded to the observer.

AI-powered digital pathology

Unstained formalin-fixed paraffin-embedded tissue slides (section thickness: 5 µm) were scanned using the Genesis® 200 system (HistoIndex, Singapore), which uses an ultrafast femtosecond laser, emitting photons to excite the unstained tissue sample at 780 nm. Second Harmonic Generation (SHG) signals at 390 nm and two-photon excited fluorescence (TPEF) signals at 550 nm were then collected at two photomultiplier tubes. The monochromic signals were colorized and subsequently merged to form SHG/TPEF image, giving a resolution of 0.39 µm/pixel. TPEF signals (red in color) provide visualization of background liver architecture while SHG signals (green color) identify collagen fibers. AI-based image analysis was performed to identify liver zone-specific 100 fibrosis features and 45 steatosis features [36], as well as the colocalization between fibrosis and steatosis [26]. Following the SHG/TPEF scanning, the same slides were stained using H&E. The whole slide images were acquired using Vectra Polaris at 40×. Inflammatory cells were detected and quantified on the H&E images using a two-stage AI pipeline that combines supervised and unsupervised approaches, based on spatial

Biochemical Journal (2024) 481 177–190
https://doi.org/10.1042/BCJ20230422

context representation [37]. In the first stage, the H&E images were divided into patches, and evaluated with a pretrained deep-learning pipeline to obtain the centroids and categories of the cells. It integrates several independent modules, including feature extractor, cell detection, cell classification, spatial context categorization, and deep clustering. In the second stage, the segmentation of cells with StarDist [38,39] was performed and matched with the cell detection and classification results from the first stage. Inflammatory cell density (i.e. the number of inflammatory cells per unit area) was then calculated. To assess the colocalization between inflammatory cells and fibrosis, the H&E images were registered to the corresponding SHG/TPEF images. The amount of fibrosis in the vicinity of inflammatory cells was quantified.

qPCR analysis

RNA from the liver was prepared using QIAzol reagent followed by chloroform extraction (Qiagen, Germantown, MD, U.S.A.). RNA was purified using the RNeasy mini kit with a DNAse digestion (Qiagen). One microgram of RNA was converted to cDNA using SuperScript VILO cDNA Synthesis Kit (Thermo Fisher Scientific) and qPCR was performed using TaqMan Fast Advanced Master Mix on a Viia7 instrument (Applied Biosystems, Waltham, MA, U.S.A.). Taqman probes (Thermo Fisher Scientific) used to assess gene expression levels are listed in Supplemental Table S2 and Tbp was used as a housekeeping gene.

Illumina stranded total RNA prep and Novaseq sequencing

For each sample, total RNA was normalized to 100 ng before undergoing library preparation using the Illumina Stranded Total RNA Prep Ligation with Ribo-Zero Plus kit (Illumina, Foster City, CA, U.S.A.) per manufacturer's instructions. The Agilent Bioanalyzer (Agilent Technologies, Santa Clara, CA, U.S.A.) and Qubit Fluorometer (Thermo Fisher Scientific) were used to qualify and quantify libraries prior to pooling samples. Samples were sequenced on the Illumina Novaseq 6000 using 2×100 cycles, per manufacturer's instructions (Illumina).

RNA sequencing analysis

Following DNA sequencing and read mapping to the mouse GRCm39 genome, reads aligning to coding regions were retained and the number of read counts per gene was calculated. The resulting read count table was then filtered to include only genes with an FPKM value greater than or equal to one in at least half of the samples. Next, differential gene expression analysis was performed using DEseq2, and the results were visualized using ggplot2 and pheatmap libraries. Genes with a fold change >1.5 and an FDR-adjusted P-value < 0.05 were considered significant. PCA analyses were performed using the top 500 genes with the greatest variance across all samples and pathway analyses were performed across GO-biological process, GO-molecular function, GO-cellular compartment, Reactome, and WikiPathway databases using clusterprofiler. Data have been deposited within the Gene Expression Omnibus repository (GSE248273).

Statistical analysis

All data were expressed as mean ± SEM. Statistical analysis was performed with GraphPad Prism 9 (GraphPad Software, Boston, MA, U.S.A.). For multiple comparisons, one-way or two-way ANOVA with Dunnett's multiple comparison tests were used. For non-parametric analyses, Kruskal–Wallis and Dunn's multiple comparison tests were performed. Multivariable analysis was performed in R using functions housed in the stats package as previously described [40]. Briefly, independent variables were passed onto the lm function. Models were built using body weight or treatment as independent variables, either independently or together, to test for multivariable interactions. ANOVA analysis was then performed using the results of these models. Differences are marked as $^{*}P < 0.05$, $^{**}P < 0.01$, and $^{***}P < 0.001$, $^{****}P < 0.0001$.

Data Availability

The authors agree to make any materials, data, code, and associated protocols available upon request. RNA-sequencing data have been deposited in GEO and can be accessed using GSE248273.

Competing Interests

All authors are employees and stockholders of Merck & Co., Inc.

PORTLAND PRESS

CRediT Author Contribution

Saswata Talukdar: Conceptualization, Resources, Supervision, Writing — original draft, Project administration, Writing — review and editing. **Erin Coyne**: Conceptualization, Formal analysis, Validation, Visualization, Methodology, Writing — original draft, Writing — review and editing. **Yilin Nie**: Investigation, Methodology. **Desiree Abdurrachim**: Resources, Software, Visualization, Methodology. **Charlene Lin Zhi Ong**: Software, Visualization, Methodology. **Yongqi Zhou**: Software, Visualization, Methodology. **Asad Abu Bakar Ali**: Resources, Software, Methodology. **Stacey Meyers**: Data curation, Methodology. **Jeff Grein**: Data curation, Software, Formal analysis. **Wendy Blumenschein**: Data curation, Software, Visualization, Methodology. **Brendan Gongol**: Data curation, Software, Methodology. **Yang Liu**: Software, Formal analysis, Visualization, Methodology. **Cedric Lorenz Hugelshofer**: Resources, Methodology. **Ester Carballo-Jane**: Data curation, Methodology.

Acknowledgements

The authors wish to acknowledge Sam Engel for critical reading and providing scientific inputs into the manuscript. The authors wish to acknowledge Yu Hsuan Lin, John Barr, Qiong Zhou, Weifeng Dong, and Salomon Martinez for advice and technical expertise. The authors wish to acknowledge Frank Liu, Kristine Devito, Carlos Rodriguez, George Boykow, Xun Chen, Andrea Nawrocki, and Sandra Souza for early characterization of BLT1i.

Abbreviations

AI, artificial intelligence; ALT, alanine transaminase; AST, aspartate transaminase; BLT1, leukotriene B4 receptor 1; CDAA–HFD, choline-deficient, L-amino acid-defined, high-fat diet; CRN, Clinical Research Network; CV, central vein; FPKM, fragments per kilobase of transcript per million mapped reads; H&E, hematoxylin and eosin; LTA4H, leukotriene A4 hydrolase; LTB4, leukotriene B4; MAS, MASLD activity score; MASH, metabolic dysfunction-associated steatohepatitis; MASLD, metabolic dysfunction-associated steatotic liver disease; PCA, principal component analysis; PS, perisinusoidal region; PSR, picrosirius red; SHG, second harmonic generation; TPEF, two-photon excited fluorescence; VEH, vehicle.

References

1 Riazi, K., Azhari, H., Charette, J.H., Underwood, F.E., King, J.A., Afshar, E.E. et al. (2022) The prevalence and incidence of NAFLD worldwide: a systematic review and meta-analysis. *Lancet Gastroenterol. Hepatol.* **7**, 851–861 https://doi.org/10.1016/S2468-1253(22)00165-0

2 Wong, V.W., Ekstedt, M., Wong, G.L. and Hagström, H. (2023) Changing epidemiology, global trends and implications for outcomes of NAFLD. *J. Hepatol.* **79**, 842–852 https://doi.org/10.1016/j.jhep.2023.04.036

3 Brunt, E.M., Wong, V.W., Nobili, V., Day, C.P., Sookoian, S., Maher, J.J. et al. (2015) Nonalcoholic fatty liver disease. *Nat. Rev. Dis. Primers* **1**, 15080 https://doi.org/10.1038/nrdp.2015.80

4 Rinella, M.E. (2015) Nonalcoholic fatty liver disease: a systematic review. *J. Am. Med. Assoc.* **313**, 2263–2273 https://doi.org/10.1001/jama.2015.5370

5 Sheka, A.C., Adeyi, O., Thompson, J., Hameed, B., Crawford, P.A. and Ikramuddin, S. (2020) Nonalcoholic steatohepatitis: a review. *J. Am. Med. Assoc.* **323**, 1175–1183 https://doi.org/10.1001/jama.2020.2298

6 Simon, T.G., Roelstraete, B., Khalili, H., Hagström, H. and Ludvigsson, J.F. (2021) Mortality in biopsy-confirmed nonalcoholic fatty liver disease: results from a nationwide cohort. *Gut* **70**, 1375–1382 https://doi.org/10.1136/gutjnl-2020-322786

7 Paik, J.M., Henry, L., De Avila, L., Younossi, E., Racila, A. and Younossi, Z.M. (2019) Mortality related to nonalcoholic fatty liver disease is increasing in the United States. *Hepatol. Commun.* **3**, 1459–1471 https://doi.org/10.1002/hep4.1419

8 Heyens, L.J.M., Busschots, D., Koek, G.H., Robaeys, G. and Francque, S. (2021) Liver fibrosis in non-alcoholic fatty liver disease: from liver biopsy to non-invasive biomarkers in diagnosis and treatment. *Front. Med.* **8**, 615978 https://doi.org/10.3389/fmed.2021.615978

9 Schuster, S., Cabrera, D., Arrese, M. and Feldstein, A.E. (2018) Triggering and resolution of inflammation in NASH. *Nat. Rev. Gastroenterol. Hepatol.* **15**, 349–364 https://doi.org/10.1038/s41575-018-0009-6

10 Chalasani, N., Abdelmalek, M.F., Garcia-Tsao, G., Vuppalanchi, R., Alkhouri, N., Rinella, M. et al. (2020) Effects of belapectin, an inhibitor of galectin-3, in patients with nonalcoholic steatohepatitis with cirrhosis and portal hypertension. *Gastroenterology* **158**, 1334–1345.e5 https://doi.org/10.1053/j.gastro.2019.11.296

11 Anstee, Q.M., Neuschwander-Tetri, B.A., Wai-Sun Wong, V., Abdelmalek, M.F., Rodriguez-Araujo, G., Landgren, H. et al. (2024) Cenicriviroc lacked efficacy to treat liver fibrosis in nonalcoholic steatohepatitis: AURORA phase III randomized study. *Clin. Gastroenterol. Hepatol.* **22**, 124–134 https://doi.org/10.1016/j.cgh.2023.04.003

12 Harrison, S.A., Wong, V.W., Okanoue, T., Bzowej, N., Vuppalanchi, R., Younes, Z. et al. (2020) Selonsertib for patients with bridging fibrosis or compensated cirrhosis due to NASH: results from randomized phase III STELLAR trials. *J. Hepatol.* **73**, 26–39 https://doi.org/10.1016/j.jhep.2020.02.027

13 Harrison, S.A., Abdelmalek, M.F., Caldwell, S., Shiffman, M.L., Diehl, A.M., Ghalib, R. et al. (2018) Simtuzumab is ineffective for patients with bridging fibrosis or compensated cirrhosis caused by nonalcoholic steatohepatitis. *Gastroenterology* **155**, 1140–1153 https://doi.org/10.1053/j.gastro.2018.07.006

Biochemical Journal (2024) **481** 177–190
https://doi.org/10.1042/BCJ20230422

14 He, R., Chen, Y. and Cai, Q. (2020) The role of the LTB4-BLT1 axis in health and disease. *Pharmacol. Res.* **158**, 104857 https://doi.org/10.1016/j.phrs.2020.104857
15 Liu, X., Wang, K., Wang, L., Kong, L., Hou, S., Wan, Y. et al. (2023) Hepatocyte leukotriene B4 receptor 1 promotes NAFLD development in obesity. *Hepatology* **78**, 562–577 https://doi.org/10.1002/hep.32708
16 Remmerie, A., Martens, L., Thoné, T., Castoldi, A., Seurinck, R., Pavie, B. et al. (2020) Osteopontin expression identifies a subset of recruited macrophages distinct from Kupffer cells in the fatty liver. *Immunity* **53**, 641–657.e14 https://doi.org/10.1016/j.immuni.2020.08.004
17 Li, P., Oh, D.Y., Bandyopadhyay, G., Lagakos, W.S., Talukdar, S., Osborn, O. et al. (2015) LTB4 promotes insulin resistance in obese mice by acting on macrophages, hepatocytes and myocytes. *Nat. Med.* **21**, 239–247 https://doi.org/10.1038/nm.3800
18 Spite, M., Hellmann, J., Tang, Y., Mathis, S.P., Kosuri, M., Bhatnagar, A. et al. (2011) Deficiency of the leukotriene B4 receptor, BLT-1, protects against systemic insulin resistance in diet-induced obesity. *J. Immunol.* **187**, 1942–1949 https://doi.org/10.4049/jimmunol.1100196
19 Callegari, I.O.M. and Oliveira, A.G. (2022) The role of LTB4 in obesity-induced insulin resistance development: an overview. *Front. Endocrinol.* **13**, 848006 https://doi.org/10.3389/fendo.2022.848006
20 Han, Y., Lim, J., Siliphaivanh, P., Spencer, K. and Tummanapalli, S. (2017) Aryl sulfonamides as BLT1 antagonists. Patent WO 2017/095724
21 Han, Y., Siliphaivanh, P., Spencer, K. and Tummanapalli, S. (2017) Aryl sulfonamides as BLT1 antagonists. Patent WO 2017/095725
22 Lefere, S., Puengel, T., Hundertmark, J., Penners, C., Frank, A.K., Guillot, A. et al. (2020) Differential effects of selective- and pan-PPAR agonists on experimental steatohepatitis and hepatic macrophages. *J. Hepatol.* **73**, 757–770 https://doi.org/10.1016/j.jhep.2020.04.025
23 Puri, P. and Sanyal, A.J. (2012) Nonalcoholic fatty liver disease: definitions, risk factors, and workup. *Clin. Liver Dis.* **1**, 99–103 https://doi.org/10.1002/cld.81
24 Kleiner, D.E., Brunt, E.M., Van Natta, M., Behling, C., Contos, M.J., Cummings, O.W. et al. (2005) Design and validation of a histological scoring system for nonalcoholic fatty liver disease. *Hepatology* **41**, 1313–1321 https://doi.org/10.1002/hep.20701
25 Wang, X.X., Jin, R., Li, X.H., Yang, Q., Teng, X., Liu, F.F. et al. (2023) Collagen co-localized with macrovesicular steatosis better differentiates fibrosis progression in non-alcoholic fatty liver disease mouse models. *Front. Med.* **10**, 1172058 https://doi.org/10.3389/fmed.2023.1172058
26 Naoumov, N.V., Brees, D., Loeffler, J., Chng, E., Ren, Y., Lopez, P. et al. (2022) Digital pathology with artificial intelligence analyses provides greater insights into treatment-induced fibrosis regression in NASH. *J. Hepatol.* **77**, 1399–1409 https://doi.org/10.1016/j.jhep.2022.06.018
27 Matsumoto, M., Hada, N., Sakamaki, Y., Uno, A., Shiga, T., Tanaka, C. et al. (2013) An improved mouse model that rapidly develops fibrosis in non-alcoholic steatohepatitis. *Int. J. Exp. Pathol.* **94**, 93–103 https://doi.org/10.1111/iep.12008
28 Zhang, X., Li, S., Zhou, Y., Su, W., Ruan, X., Wang, B. et al. (2017) Ablation of cytochrome P450 omega-hydroxylase 4A14 gene attenuates hepatic steatosis and fibrosis. *Proc. Natl Acad. Sci. U. S. A.* **114**, 3181–3185 https://doi.org/10.1073/pnas.1700172114
29 Li, S., Wang, C., Zhang, X. and Su, W. (2021) Cytochrome P450 omega-hydroxylase 4a14 attenuates cholestatic liver fibrosis. *Front. Physiol.* **12**, 688259 https://doi.org/10.3389/fphys.2021.688259
30 Guo, Y., Miao, X., Sun, X., Li, L., Zhou, A., Zhu, X. et al. (2023) Zinc finger transcription factor Egf1 promotes non-alcoholic fatty liver disease. *JHEP Rep.* **5**, 100724 https://doi.org/10.1016/j.jhepr.2023.100724
31 Kim, K.H., Kim, S.H., Han, D.H., Jo, Y.S., Lee, Y.H. and Lee, M.S. (2018) Growth differentiation factor 15 ameliorates nonalcoholic steatohepatitis and related metabolic disorders in mice. *Sci. Rep.* **8**, 6789 https://doi.org/10.1038/s41598-018-25098-0
32 Wang, Y., Chen, C., Chen, J., Sang, T., Peng, H., Lin, X. et al. (2022) Overexpression of NAG-1/GDF15 prevents hepatic steatosis through inhibiting oxidative stress-mediated dsDNA release and AIM2 inflammasome activation. *Redox Biol.* **52**, 102322 https://doi.org/10.1016/j.redox.2022.102322
33 Im, Y.R., Hunter, H., de Gracia Hahn, D., Duret, A., Cheah, Q., Dong, J. et al. (2021) A systematic review of animal models of NAFLD finds high-fat, high-fructose diets most closely resemble human NAFLD. *Hepatology* **74**, 1884–1901 https://doi.org/10.1002/hep.31897
34 Huby, T. and Gautier, E.L. (2022) Immune cell-mediated features of non-alcoholic steatohepatitis. *Nat. Rev. Immunol.* **22**, 429–443 https://doi.org/10.1038/s41577-021-00639-3
35 Sanyal, A.J., Chalasani, N., Kowdley, K.V., McCullough, A., Diehl, A.M., Bass, N.M. et al. (2010) Pioglitazone, vitamin E, or placebo for nonalcoholic steatohepatitis. *N. Engl. J. Med.* **362**, 1675–1685 https://doi.org/10.1056/NEJMoa0907929
36 Liu, F., Goh, G.B., Tiniakos, D., Wee, A., Leow, W.Q., Zhao, J.M. et al. (2020) qFIBS: an automated technique for quantitative evaluation of fibrosis, inflammation, ballooning, and steatosis in patients with nonalcoholic steatohepatitis. *Hepatology* **71**, 1953–1966 https://doi.org/10.1002/hep.30986
37 Abousamra, S., Belinsky, D., Van Arnam, J., Allard, F., Yee, E., Gupta, R. et al. (2021) *Multi-class cell detection using spatial context representation*. In *Proceedings of the IEEE CVF International Conference on Computer Vision, 11-17 October 2021*, IEEE, Montreal, QC, Canada, pp. 4005–4014 https://doi.org/10.1109/ICCV48922.2021.00397
38 Schmidt, U., Wiet, M., Broaddus, C. and Myers, G. (2018) Cell detection with star-convex polygons. In *Medical Image Computing and Computer Assisted Intervention* (Frangi, A., Schnabel, J., Davatzikos, C., Alberola-López, C., Fichtinger, G., eds), vol. **11071**, pp. 265–273, Springer, Cham
39 Weigert, M., Shit, U., Haase, R., Sugawara, K. and Myers, G. (2020) *Star-convex polyhedra for 3D object detection and segmentation in microscopy*. In *Proceedings of the IEEE CVF Winter Conference on Applications of Computer Vision, 1-5 March 2020*, IEEE, Snowmass Village, CO, USA, pp. 3666–3673 https://doi.org/10.1109/WACV45572.2020.9093435
40 Skinner, J. (2018) Statistics for immunologists. *Curr. Protoc. Immunol.* **122**, 54 https://doi.org/10.1002/cpim.54